

See discussions, stats, and author profiles for this publication at: <https://www.researchgate.net/publication/231235713>

# X-ray Diffraction, XPS, and Magnetic Properties of Lanthanide-Based Misfit-Layered Sulfides Intercalated with Cobaltocene

ARTICLE *in* CHEMISTRY OF MATERIALS · NOVEMBER 2000

Impact Factor: 8.35 · DOI: 10.1021/cm0010396

CITATIONS

6

READS

21

6 AUTHORS, INCLUDING:



**Luis Sánchez**

University of Cordoba (Spain)

93 PUBLICATIONS 1,641 CITATIONS

SEE PROFILE



**Jesús Santos-Peña**

University of Tours

57 PUBLICATIONS 799 CITATIONS

SEE PROFILE



**Enrique Rodríguez-Castellón**

University of Malaga

397 PUBLICATIONS 5,322 CITATIONS

SEE PROFILE

# X-ray Diffraction, XPS, and Magnetic Properties of Lanthanide-Based Misfit-Layered Sulfides Intercalated with Cobaltocene

L. Hernan,<sup>†</sup> J. Morales,<sup>\*,†</sup> L. Sánchez,<sup>†</sup> J. Santos,<sup>†</sup> E. Rodríguez-Castellón,<sup>‡</sup> and J. L. Martínez<sup>§</sup>

*Departamento de Química Inorgánica, Facultad de Ciencias, Universidad de Córdoba, Campus de Rabanales, Edificio C-3, E-14071 Córdoba, Spain, Departamento de Química Inorgánica, Facultad de Ciencias, Universidad de Málaga, Málaga, Spain, and Instituto de Ciencias de Materiales de Madrid, CSIC, Cantoblanco, Madrid, Spain*

*Received March 17, 2000. Revised Manuscript Received September 19, 2000*

Polycrystalline  $(\text{CeS})_{1.15}(\text{TaS}_2)_2$  and  $(\text{SmS})_{1.19}(\text{TaS}_2)_2$ , two composite misfit-layered sulfides, react directly with cobaltocene ( $\text{CoCp}_2$ ) in acetonitrile solutions to form novel intercalation compounds of composition  $(\text{CeS})_{1.15}(\text{TaS}_2)_2(\text{CoCp}_2)_{0.31}$  and  $(\text{SmS})_{1.19}(\text{TaS}_2)_2(\text{CoCp}_2)_{0.30}$ , respectively. Their powder X-ray diffraction data reveal a significant expansion (ca. 5.5 Å) along the  $c$ -axis and preservation of the  $a$ - $b$ -axis dimensions. One-dimensional electron density calculations are consistent with a model where the guest molecule is located at all  $\text{TaS}_2$ - $\text{TaS}_2$  interfaces, whereas  $\text{MS}$ - $\text{TaS}_2$  ( $\text{M} = \text{Ce}, \text{Sm}$ ) interfaces remain empty. The Ce and Sm 3d core-level spectra reveal that these elements are present mainly as tervalent ions. The magnetic properties of the Ce compound are consistent with this valence state. Although the intercalation of cobaltocene does not shift the binding energies of the host constituent elements appreciably, the organometallic molecule is intercalated as  $\text{CoCp}_2^+$  ions, as is usually the case with layered chalcogenide hosts. In the case of the Ce system, this model is also supported by the magnetic data and suggests that the electron donated by the guest molecule is transferred to the conduction band of the  $\text{TaS}_2$  layers, whereas the lanthanide element remains as a trivalent ion. The formal electron transfer apparently taking place from the  $\text{MS}$  bilayer ( $\text{M} = \text{Ce}, \text{Sm}$ ) to  $\text{TaS}_2$  sheets does not prevent ionization of cobaltocene.

## Introduction

Recently, we demonstrated the high potential of misfit-layered sulfides of formula  $(\text{PbS})_{1+x}(\text{TS}_2)_2$  ( $\text{T} = \text{Ti}, \text{Ta}$ ) as host lattices for atomic and molecular electron-donor guest species.<sup>1</sup> This outstanding property is believed to rely on two salient facts, namely, (a) the presence in their structures of an interlayer region at the interface between two consecutive close-packed sulfur atom layers, available to accommodate the guest species<sup>2</sup> and (b) the very limited electron transfer from the  $\text{PbS}$  sublattice to the  $\text{TS}_2$  sheet, which allows the  $\text{TS}_2$  part to accept charge transferred from the guest. It is also well documented from spectroscopic techniques, electrical transport, and magnetic properties<sup>2</sup> that the electron donation from the  $\text{MS}$  part to the  $\text{TS}_2$  one significantly increases when  $\text{M}$  is a lanthanide. In fact, this phenomenon has been considered the main

reason for the lack of intercalation in  $\text{SmNb}_2\text{S}_5$  treated with lithium or sodium derivatives,<sup>3</sup> although the monolayer misfit compound  $(\text{SmS})_{1+x}\text{TaS}_2$  can be formally considered an intercalation compound of the bilayer misfit compound  $(\text{SmS})_{1+x}(\text{TaS}_2)_2$  and  $\text{SmS}$  whereby charge transfer occurs from  $\text{SmS}$  toward  $\text{TaS}_2$  layers. In any case, the bilayer compound cannot be obtained by direct synthesis from the monolayer one and  $\text{SmS}$ . By contrast, the bilayer misfit compound  $\text{PbNb}_2\text{S}_5$  easily intercalates Li or Na when exposed to  $n$ -butyllithium or sodium naphthalide, respectively.<sup>3,4</sup> Although recent reports on the preparation of  $\text{Cu}_y(\text{MS})_{1+x}(\text{NbS}_2)_2$  ( $\text{M} = \text{Ce}, \text{Sm}$ )<sup>5</sup> and  $\text{E}_y(\text{MS})_{1+x}(\text{TiS}_2)_2$  ( $\text{E} = \text{Fe}, \text{Ni}$ ;  $\text{M} = \text{La}, \text{Ce}$ )<sup>6</sup> intercalates question the adequacy of lanthanide-based misfit-layered sulfides as host lattices for intercalation compounds, the above-mentioned intercalates have been obtained by direct synthesis from the elements at high temperatures, an unusual method for preparing intercalation compounds taking into account that most of them are metastable phases. Some discrepancies exist among reported interlayer expansions

\* Corresponding author. E-mail: iq1mopaj@uco.es.

<sup>†</sup> Universidad de Córdoba.

<sup>‡</sup> Universidad de Málaga.

<sup>§</sup> CSIC.

(1) Hernán, L.; Morales, J.; Sánchez, L.; Tirado, J. L. *Chem. Mater.* **1993**, *5*, 1167. Hernán, L.; Morales, J.; Santos, J.; Espínos, J. P.; González Elipe, A. R. *J. Mater. Chem.* **1998**, *8*, 2281. Hernán, L.; Morales, J.; Santos, J. *J. Solid State Chem.* **1998**, *141*, 323.

(2) Wieggers, G. A.; Meerschaut, A. Sandwiched Incommensurate Layered Compounds. In *Non-Commensurate Layered Compounds*; Meerschaut, A., Ed.; Trans. Tech. Pub. Ltd.: Zurich, 1992. Wieggers, G. A. *Prog. Solid State Chem.* **1996**, *1*, 24 and references therein.

(3) Bonneau, P.; Mansot, J. L.; Rouxel, J. *Mater. Res. Bull.* **1993**, *28*, 757.

(4) Hernán, L.; Lavela, P.; Morales, J.; Pattanayak, J.; Tirado, J. L. *Mater. Res. Bull.* **1991**, *26*, 1211.

(5) Ohno, Y. *J. Solid State Chem.* **1997**, *134*, 99; *Phys. Rev. B* **1996**, *54*, 11693.

(6) Suzuki, K.; Nakamura, O.; Kondo, T.; Enoki, T. *J. Phys. Chem. Solids* **1996**, *57*, 1133.

that are critical with a view to assessing the formation of an intercalate. Thus, while the interlayer distance increases by 0.62 Å with Cu intercalation, the expansion is negligible in Fe and Ni intercalates. In this article, we demonstrate for the first time that, like lead-based misfit-layered sulfides,<sup>7</sup> lanthanide-based misfit-layered sulfides can intercalate large electron donor molecules such as cobaltocene under mild experimental conditions ("chimie douce" methods). The new complexes thus prepared contradict the belief that it is virtually impossible for electron donor species in (MS)<sub>1+x</sub>(TS<sub>2</sub>)<sub>2</sub> to give intercalation reactions when M is a lanthanide<sup>3</sup> and suggest that electronic factors such as electron transfer from the MS part to the TS<sub>2</sub> slab play a more modest role than one would have expected.

### Experimental Section

Two misfit-layered sulfides, (MS)<sub>1+x</sub>(TaS<sub>2</sub>)<sub>2</sub> (M = Ce, Sm), were tested as host lattices. The Ce compound was prepared by direct synthesis from the elements as described elsewhere.<sup>8</sup> The Sm compound was obtained by heating a mixture of Sm<sub>2</sub>S<sub>3</sub>, Ta, and S (supplied by Strem Chem.) in a mole proportion of 1.19:2.5:1.9 in an evacuated silica tube. The mixture was heated at 450 °C for 1 day and then at 950 °C for 7 days. The pellet was ground and heated at 950 °C for another 7 days. The tubes were opened in a drybox (Mbraun 250), and the crystals were manually ground in an agata mortar.

Inside the glovebox, the crystalline hosts were added to a solution of CoCp<sub>2</sub>, in dry acetonitrile, supplied by Strem Chem. About 400 mg of the host was mixed with 4 mL of 0.1 M CoCp<sub>2</sub> solution. The reaction was carried out in evacuated and sealed Pyrex tubes at 90 °C, previously frozen under liquid nitrogen and evacuated to  $P < 10^{-3}$  mbar. A period of 4 days was found to be long enough to obtain 100% conversion. The absence of (00 $l$ ) reflections from the host was taken as evidence of thorough intercalation. The tubes were opened in the drybox and the intercalates washed with acetonitrile and stored under Ar in sealed glass tubes until their characterization. The amount of intercalant was determined by combining the results of the elemental analysis carried out on a Fisons CHNS analyzer with those of atomic absorption spectroscopy for calculation of the cobalt content.

Powder X-ray diffraction (XRD) patterns were recorded on a Siemens D5000 powder diffractometer using Cu K $\alpha$  radiation and operating at 40 kV and 30 mA; the diffracted beam was made monochromatic by using a graphite monochromator. For identification purposes, intensities were collected at 0.02° (2 $\theta$ ) intervals, using 0.06 s/step. For evaluation of lattice parameters and one-dimensional Patterson function calculations,<sup>9</sup> intensities were recorded in the same scan step, at 3.6 s/step. To avoid contact of the intercalated products with moisture, XRD patterns were obtained by covering the sample holder with a plastic film under an argon atmosphere. Unit cell dimensions were obtained by the least-squares procedures, using between 15 and 20 reflections to determine each subcell. One-dimensional electron-density maps were obtained by using 15 (00 $l$ ) reflections for pristine compounds and 13 (00 $l$ ) reflections for intercalates that were selected in such a way as to avoid overlap with other ( $hkl$ ) reflections. Intensities ( $I$ ) were obtained from integrated peak areas. The structure factors,  $F$ , of these reflections were obtained from their intensities by using the following equation:

$$|F(I)| = (I/Lp)^2 \quad (1)$$

where  $Lp$  is the Lorentz-polarization factor as calculated from the equation  $Lp = (1 + \cos^2 2\theta)/\sin^2 \theta \cos \theta$ . Structure factors were phased by calculating a value for each  $F_{00l}$  from the atomic factors and assumed position of each atom. The positions used were those of metal and sulfur coordinates obtained for orthorhombic (PbS)<sub>1.14</sub>(NbS<sub>2</sub>)<sub>2</sub> from single-crystal X-ray data<sup>10</sup> as no X-ray single-crystal structures for lanthanide-based bilayer compounds have so far been reported. 1-D electron densities were obtained from the following equation:

$$\rho(z) = 1/L \sum F_{00l} \cos(2\pi lz) \quad (2)$$

where  $L$  is the lattice periodicity.

XPS spectra were obtained by using a Physical Electronics PHI 700 spectrometer with nonmonochromatic Mg K $\alpha$  as excitation source (300 W, 15 kV, 1253.6 eV). Samples, made into pellets by compressing the powdered compounds at about 3 tonnes under an argon atmosphere, were rapidly mounted on a sample holder without adhesive tape and immediately transferred to the spectrometer's preparation chamber, where they were kept overnight at high vacuum before they were transferred to the spectrometer analysis chamber. The PHI ACCESS ESCA-V6.0 software package was used for data acquisition and analysis. Recorded spectra were always fitted using Gauss-Lorentz curves in order to more accurately determine the binding energy of the different element core levels. The S 2p signal at 161.7 eV was used as reference<sup>7,11</sup> since this element is shared by the studied compounds. Magnetic susceptibility was measured by using a commercially available SQUID magnetometer over the temperature range 1.7–300 K under an applied magnetic field ranging from 0.5 to 5 kOe.

### Results and Discussion

The X-ray diffraction patterns for the Ce and Sm sulfides are shown in Figure 1a,b. One common feature of both compounds is the presence of a set of narrow multiple-order reflections (00 $l$ ) of high intensity with additional broad, weak lines, all of which suggests a coherent structure with a long range (at least along the  $c$ -axis) and in-plane defects and inhomogeneities owing to the incommensurability along  $a$ -axis direction. Like those for the monolayer compounds (CeS)<sub>1.15</sub>TaS<sub>2</sub><sup>12</sup> and (SmS)<sub>1.19</sub>TaS<sub>2</sub>,<sup>13</sup> the spectra were indexed in the orthorhombic system. The unit cell dimensions of both sublattices are given in Table 1. The values for the  $c$ -axis confirm that these compounds belong to the bilayer family and that the repeat unit consists of two consecutive TaS<sub>2</sub> slabs and one MS slab stacked along the  $c$ -axis. From the  $2a_{\text{TaS}_2}/a_{\text{MS}}$  ratio, the stoichiometries (CeS)<sub>1.15</sub>(TaS<sub>2</sub>)<sub>2</sub> and (SmS)<sub>1.19</sub>(TaS<sub>2</sub>)<sub>2</sub> were derived. The subindices of the MS sublattices coincide with those of the monolayer compounds; those for the Ce compound, however, differ slightly from the ones reported by Suzuki et al.<sup>8</sup> (1.12). These authors only calculated the interlayer spacing, which was somewhat larger (17.45 Å) than the  $c$ -axis dimension given in Table 1.

(9) Klug, H. P.; Alexander, L. E. *X-ray Diffraction Procedures for Polycrystalline and Amorphous Materials*; Wiley: New York, 1974; p 135.

(10) Meerschaut, A.; Guemas, L.; Auriel, C.; Rouxel, J. *Eur. J. Solid State Inorg. Chem.* **1990**, 27, 557.

(11) Wagner, C. D.; Riggs, W. M.; Davis, L. E.; Moulder, J. E.; Muilenberg, G. E. *Handbook of X-ray Photoelectron Spectroscopy*; Perkin-Elmer, Physical Electronics Division: Eden Prairie, MN, 1978.

(12) Wiegiers, G. A.; Meetsma, A.; Haange, R. J.; de Boer, J. L. *J. Less-Common Met.* **1991**, 68, 347.

(13) de Boer, J. L.; Meetsma, A.; Zeinstra, Th. J.; Haange, R. J.; Wiegiers, G. A. *Acta Crystallograph* **1991**, C47, 924.

(7) Hernán, L.; Morales, J.; Sánchez, L.; Tirado, J. L.; González Elípe, A. R. *J. Chem. Soc., Chem. Commun.* **1994**, 1081. Hernán, L.; Morales, J.; Sánchez, L.; Tirado, J. L.; Espinós, J. P.; González-Elípe, A. R. *Chem. Mater.* **1995**, 7, 1576.

(8) Suzuki, K.; Kojima, N.; Ban, T.; Tsujikawa, Y. *J. Phys. Soc. Jpn.* **1990**, 59, 266.

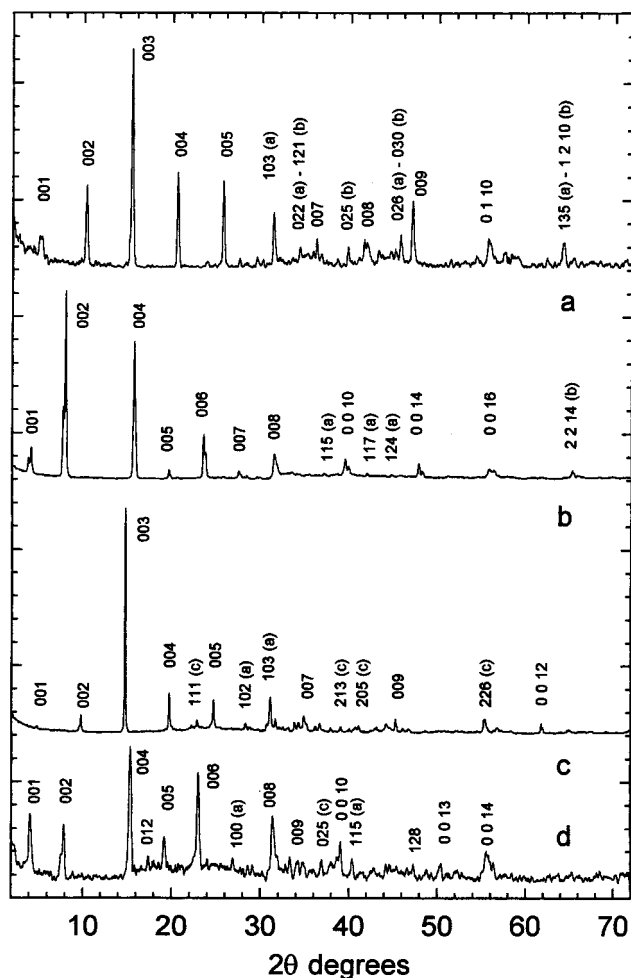


**Figure 1.** XRD patterns for (a)  $(\text{CeS})_{1.15}(\text{Ta}_2\text{S}_2)_2$ , (b)  $(\text{CeS})_{1.15}-(\text{Ta}_2\text{S}_2)_2(\text{CoCp}_2)_{0.31}$ , (c)  $(\text{SmS})_{1.19}(\text{Ta}_2\text{S}_2)_2$ , and (d)  $(\text{SmS})_{1.19}(\text{Ta}_2\text{S}_2)_2-(\text{CoCp}_2)_{0.30}$ . Key: (a)  $\text{TaS}_2$  subsystem; (b) CeS subsystem; (c) SmS subsystem.

**Table 1. Lattice Constants for Misfit-Layered Sulfides and Their Cobaltocene Intercalates**

compd	subcell	<i>a</i> (Å)	<i>b</i> (Å)	<i>c</i> (Å)
$(\text{CeS})_{1.15}(\text{Ta}_2\text{S}_2)_2$	CeS	5.717(8)	5.745(7)	17.31(4)
	Ta <sub>2</sub> S <sub>2</sub>	3.288(2)	5.747(8)	17.35(2)
$(\text{CeS})_{1.15}(\text{Ta}_2\text{S}_2)_2(\text{CoCp}_2)_{0.31}$	CeS	5.741(8)	5.745(7)	22.84(2)
	Ta <sub>2</sub> S <sub>2</sub>	3.289(5)	5.744(4)	22.82(4)
$(\text{SmS})_{1.19}(\text{Ta}_2\text{S}_2)_2$	SmS	5.566(7)	5.680(8)	17.98(2)
	Ta <sub>2</sub> S <sub>2</sub>	3.285(4)	5.671(9)	17.99(4)
$(\text{SmS})_{1.19}(\text{Ta}_2\text{S}_2)_2(\text{CoCp}_2)_{0.30}$	SmS	5.549(3)	5.683(7)	23.51(1)
	Ta <sub>2</sub> S <sub>2</sub>	3.293(8)	5.677(3)	23.53(4)

The cobaltocene contents of the intercalates are shown in Table 2, together with their nitrogen and sulfur contents. The negligible N contents obtained provide direct evidence for the absence of solvent ( $\text{CH}_3\text{CN}$ ) inclusion during intercalation; on the other hand, the sulfur contents changed very little (differences between experimental and calculated percentages were within the experimental error of the analytical technique). It is worth noting that these intercalates have cobaltocene contents similar to those found in lead-based misfit bilayer sulfides,<sup>7</sup> which suggests that geometric factors play a crucial role in the intercalation reaction. The XRD patterns for the intercalates, Figure 1b,d, maintain some of the characteristic features of those for the pristine compounds, namely the presence of prominent peaks with several harmonics, all belonging to (00/)

specular reflections and smaller peaks that account for (*hkl*) reflections. However, the former set of reflections exhibits two salient differences: (i) a change in the intensities of (00/)*l* reflections relative to other (*hkl*) reflections due to the preferred orientation of particles, which is indicative of the nature of the layered structure; (ii) shifts in the  $2\theta$  angle to lower values. Like those for the parent compounds, the patterns were indexed in the orthorhombic system. The unit cell parameters for both sublattices are shown in Table 1. Note that the  $2a_{\text{Ta}_2\text{S}_2}/a_{\text{MS}}$  ratio and the *a* and *b* axes hardly change upon intercalation, which indicates that the host stoichiometry is preserved and that layers in the *ab* plane are scarcely distorted. However, significant expansion (about 5.5 Å/MS-TaS<sub>2</sub>-TaS<sub>2</sub> unit packing) was observed in both intercalates. Such an expansion is typical of simple unsubstituted metallocenes in binary<sup>14</sup> and ternary chalcogenides<sup>7</sup> and suggests that the cobaltocene molecule is located at all TaS<sub>2</sub>-TaS<sub>2</sub> interlayers and leaves MS-TaS<sub>2</sub> interlayers empty.

Additional evidence in support of this model is provided by the one-dimensional electron density functions calculated from (00/)*l* reflections. The one-dimensional electron density functions of the original and intercalated compounds, referred to the Sm system, are shown in Figure 2. As expected, the projection of the structure of the original compound on the *c*-axis gives strong peaks that can be assigned to the layers involving the heaviest atoms (viz. the Ta layers and SmS slices); on the other hand, the smaller peaks correspond to the layers of sulfur atoms. As can also be seen from Figure 2a, there is no electron density between the two consecutive sulfur layers (between 8.1 and 9.7 Å), which correspond to the van der Waals gap in  $(\text{SmS})_{1.19}(\text{Ta}_2\text{S}_2)_2$ . The one-dimensional electron density map for  $(\text{SmS})_{1.19}-(\text{Ta}_2\text{S}_2)_2(\text{CoCp}_2)_{0.30}$ , Figure 2b, was obtained by incorporating the guest molecule into the model with the cobalt atom at  $z/c = 0.5$  and their molecular axis parallel to the host lattice layers, as commonly found in most binary chalcogenides intercalated with cobaltocene.<sup>15</sup> The cobaltocene intercalate preserves the original peaks associated with the host framework and exhibits a new, broad peak centered at 11.73 Å that can be assigned to the cobaltocene molecule. The appearance of this peak reveals that the internal structure of the misfit-layered compound remains virtually intact and that the CoCp<sub>2</sub> molecule is located at interlayer TaS<sub>2</sub>-TaS<sub>2</sub> regions rather than at SmS-TaS<sub>2</sub> interfaces.

Preliminary XPS results revealed good consistency of the Ce, Sm, and S photoemission peaks with those reported for the misfit-layered compounds CeNbS<sub>3</sub><sup>16</sup> and  $(\text{SmS})_{1.19}\text{Ta}_2\text{S}_2$ .<sup>17</sup> The Ce 3d spectrum, analyzed by fitting the curve to two peaks and assuming a Gaussian-Lorentzian profile, is shown in Figure 3a. The main peaks, located at 885.7 and 903.8 eV, correspond to 3d<sub>5/2</sub> and 3d<sub>3/2</sub> spin-orbit splitting, respectively, and can be assigned to the poorly screened 3d<sup>9</sup>4f<sup>1</sup>*v*<sup>*m*</sup> final state, where *v* denotes the electron valence. The shoulders observed on the low binding energy side of the main

(14) Dines, M. B. *Science* **1975**, *188*, 1210.

(15) Wong, H. V.; Evans, J. S. O.; Barlow, S.; Mason, S. J.; O'Hare, D. *Inorg. Chem.* **1995**, *33*, 5515. Evans, J. S. O.; O'Hare, D. *Chem. Mater.* **1995**, *7*, 1668.

(16) Ohno, Y. *Phys. Rev. B* **1993**, *48*, 5515.

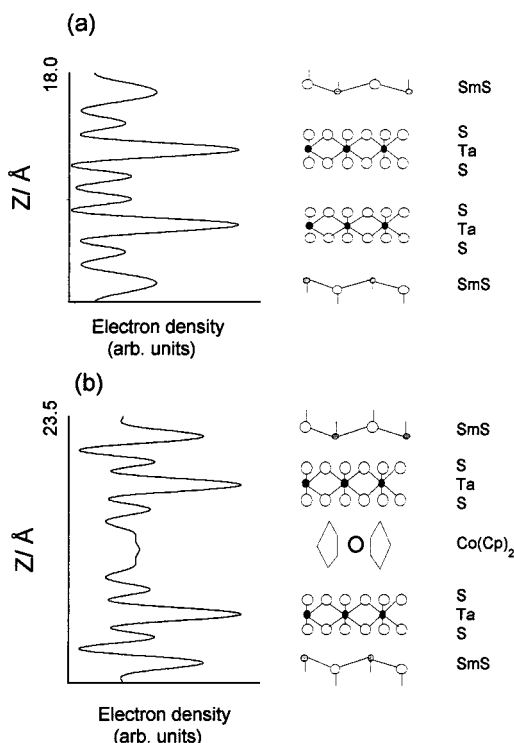
(17) Suzuki, K.; Enoki, T. *Phys. Rev. B* **1993**, *48*, 11077.



Table 2. Analytical Data (%) for Pristine and Intercalated Compounds<sup>a</sup>

compd	Co	C	H	S
(CeS) <sub>1.15</sub> (TaS <sub>2</sub> ) <sub>2</sub>				23.24 (24.03)
(CeS) <sub>1.15</sub> (TaS <sub>2</sub> ) <sub>2</sub> (CoCp <sub>2</sub> ) <sub>0.31</sub> <sup>b</sup>	2.41 (2.44)	5.03 (5.05)	0.45 (0.42)	22.12 (22.12)
(SmS) <sub>1.19</sub> (TaS <sub>2</sub> ) <sub>2</sub>				21.72 (23.52)
(SmS) <sub>1.19</sub> (TaS <sub>2</sub> ) <sub>2</sub> (CoCp <sub>2</sub> ) <sub>0.30</sub> <sup>b</sup>	2.32 (2.29)	4.55 (4.59)	0.44 (0.38)	20.34 (20.62)

<sup>a</sup> Calculated values are given in parentheses. <sup>b</sup> Negligible N content.



**Figure 2.** Electron density projection along the *c*-axis: (a) (SmS)<sub>1.19</sub>(TaS<sub>2</sub>)<sub>2</sub>; (b) (SmS)<sub>1.19</sub>(TaS<sub>2</sub>)<sub>2</sub>(CoCp<sub>2</sub>)<sub>0.30</sub>.

peaks must correspond to the well-screened  $3d^9 4f^2 v^{m-1}$  final states.<sup>16</sup> All these features are highly consistent with the presence of Ce<sup>3+</sup> as the main species. The 3d core-level Sm profile also exhibits two sets of peaks (see Figure 3b), namely, two peaks at 1083.3 and 1110.7 eV that are consistent with Sm<sup>3+</sup>  $3d_{5/2}$  and  $3d_{3/2}$ , respectively. The other two peaks are centered at 1075 and 1102.5 eV, and their position coincides with that of the Auger peaks of Ta (Ta<sub>NNN</sub>) and S (S<sub>LMN</sub>), respectively.<sup>9</sup> The Sm 3d spectrum for the precursor, Sm<sub>2</sub>S<sub>3</sub> (Figure 3c), exhibits the same features except for a decreased intensity in the peak at 1102.5 eV due to a lower S/Sm ratio. Two sets of peaks at 1083, 1110 and 1073, 1100 eV have also been found in (SmS)<sub>1.19</sub>TaS<sub>2</sub><sup>17</sup> using an Al radiation source. Under these conditions, the intensity of the peak at about 1100 eV is considerably reduced. The stronger peaks observed at 1083 and 1110 eV are assigned to Sm<sup>3+</sup>; on the other hand, the peaks at 1073 and 1110 eV are considerably weaker and assigned to Sm<sup>2+</sup> impurities. Our results question the mixed-valence state of Sm<sup>2+</sup> and Sm<sup>3+</sup> for our Sm compound and are better interpreted by assuming an unique oxidation state for Sm located in an electronic environment similar to that of Sm<sub>2</sub>S<sub>3</sub>.

The main peak in the Ta 4d core-level spectra ( $4d_{5/2}$ ) appears as a broad, asymmetric band at 226.7 eV for both compounds owing to overlap with the S 2s photoemission peak (BE = 226.1 eV). However, the Ta  $4d_{3/2}$  doublet is rather symmetric with a BE of 239.7 eV,

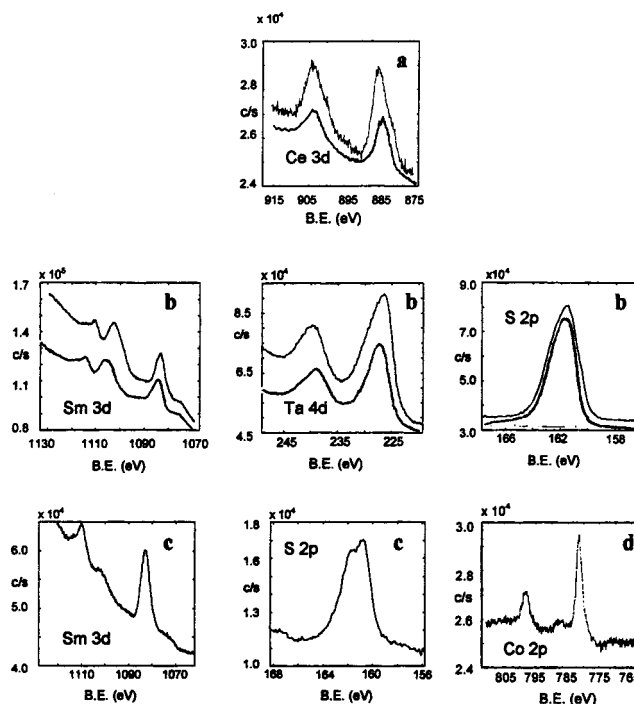


**Figure 3.** Ce 3d, Sm 3d, Ta 4d, and S 2p core-level spectra for (a) (CeS)<sub>1.15</sub>(TaS<sub>2</sub>)<sub>2</sub> (upper curve) and (CeS)<sub>1.15</sub>(TaS<sub>2</sub>)<sub>2</sub>-(CoCp<sub>2</sub>)<sub>0.31</sub> (lower curve), (b) (SmS)<sub>1.19</sub>(TaS<sub>2</sub>)<sub>2</sub> (upper curve) and (SmS)<sub>1.19</sub>(TaS<sub>2</sub>)<sub>2</sub>(CoCp<sub>2</sub>)<sub>0.30</sub> (lower curve), and (c) Sm<sub>2</sub>S<sub>3</sub>. (d) Co 2p core-level spectra for (SmS)<sub>1.19</sub>(TaS<sub>2</sub>)<sub>2</sub>(CoCp<sub>2</sub>)<sub>0.30</sub>.

which is similar to the value for lead- and tin-based misfit-layered sulfides<sup>18</sup> and consistent with the presence of a single type of Ta in the structure. Moreover, spin-orbit coupling for the S 2p photoemission peak is barely detected and appears as broad band, which might be indicative of a different chemical environment for sulfur atoms in the two sublattices, TaS<sub>2</sub> and SmS layers, forming the framework. By contrast, in Sm<sub>2</sub>S<sub>3</sub>, where S atoms are in identical chemical environments, s-o splitting is about 1.2 eV (see Figure 3c).

The Co 2p spectrum for the intercalates can be described as a main component at approximately 781.6 eV (Co 2 p<sub>3/2</sub> emission peak, Figure 3d). Although BE for Co is somewhat smaller than the values for lead-based misfit-layered sulfide intercalates,<sup>7</sup> it is shifted to higher binding energies by more than 2 eV with respect to neutral solid cobaltocene.<sup>19</sup> In other words, cobaltocene is essentially intercalated as an ionized guest species between layers, as in many other layered chalcogenide hosts.<sup>20,21</sup> Although the emission peaks of the host matrix elements become somewhat weaker

(18) Ettema, A. R. H.; Haas, C. *J. Phys. C: Condens. Matter* **1993**, 5, 3817.

(19) Barber, M.; Connors, J. A.; Derrick, L. M. R.; Hall, M. B.; Hillier, I. H. *J. Chem. Soc., Chem. Commun.* **1971**, 71.

(20) Gamble, F. R.; Thompson, A. H. *Solid State Commun.* **1978**, 27, 379.

(21) O'Hare, D. *Chem. Soc. Rev.* **1992**, 121, and references therein.

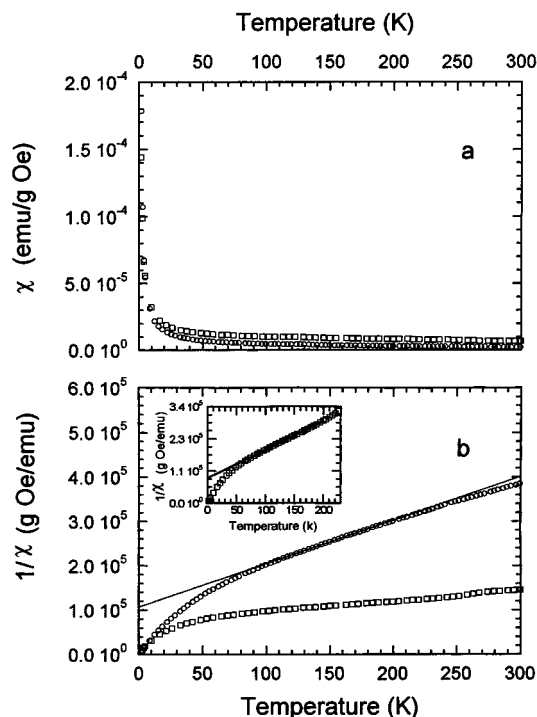


**Figure 4.** (a) Temperature dependence of the magnetic susceptibility of the Ce misfit-layered sulfide and its intercalate. (b)  $\chi^{-1}$  vs  $T$  plot. The inset shows the inverse susceptibility of the intercalate after subtraction of the temperature-independent term. Key: (○)  $(\text{CeS})_{1.15}(\text{TaS}_2)_2$ ; (□)  $(\text{CeS})_{1.15}(\text{TaS}_2)_2(\text{CoCp}_2)_{0.31}$ .

upon cobaltocene intercalation, the shifts in their binding energies are negligible (see Figure 3a,b). This behavior is consistent with previous findings for lead-based misfit-layered compounds treated with cobaltocene<sup>7</sup> and has been ascribed to the high density of states near the Fermi level that can accommodate a significant number of electrons while maintaining essentially the same electronic structure.<sup>22</sup> Nevertheless, our results contradict those for the  $\text{NiPS}_3\text{-CoCp}_2$ <sup>23</sup> and  $\text{SnS}_2\text{-CoCp}_2$ <sup>24</sup> systems, where the electron density of the host lattice shifts the 2p levels of Ni, P, and S and the 3d level of Sn toward lower energies. However, this finding cannot be generalized, as shown by the deposition and subsequent intercalation of Na in  $\text{SnS}_2$  crystals under ultrahigh-vacuum conditions. In this case, shifts in the photoelectron binding energies of the substrate are negligible.<sup>25</sup>

The magnetic susceptibility,  $\chi$ , for the Ce system was measured from 2 to 300 K, using a magnetic field of 1000 Oe. Figure 4a includes the temperature dependence of magnetic susceptibility of the pristine and intercalated compounds. The two phases show a Pauli paramagnetism owing to the conducting electrons—the compound of related composition  $(\text{CeS})_{0.6}\text{TaS}_2$  reported by Suzuki et al.<sup>8</sup> possesses metallic conductivity—and exhibit a significant contribution of a Van Vleck type paramagnetism from the CeS layers. The former con-

tribution notably increases upon intercalation. The variation of the reciprocal magnetic susceptibility of  $(\text{CeS})_{1.15}(\text{TaS}_2)_2$  and its intercalate as a function of temperature is shown in Figure 4b. The reciprocal susceptibilities do not obey the Curie–Weiss law throughout the temperature range; rather, they exhibit a convex curvature. Above 100 K, the susceptibility of the parent compound conforms fairly well to the Curie–Weiss law. The magnetic moment per cerium atom derived from the Curie constant,  $2.63 \mu_B$ , is similar to that estimated by Wiegers et al.<sup>26</sup> for  $(\text{CeS})_{1.16}\text{NbS}_2$  single crystals, with the magnetic field parallel to the layers, and to that calculated by Suzuki et al.<sup>8</sup> for the compound of nominal composition  $(\text{CeS})_{0.6}\text{TaS}_2$  ( $\mu_{\text{eff}} = 2.59 \mu_B/\text{Ce}$ ) but slightly larger than the predicted value for the  $\text{Ce}^{3+}$  free ion ( $2.54 \mu_B$ ). The discrepancy may be due to the presence of a small amount of  $\text{Ce}^{2+}$  ions and/or to the contribution of weak, temperature-independent paramagnetism associated with metallic electrons. Extrapolation of the reciprocal susceptibility yields a negative value (about  $-129$  K) for the Weiss constant. At lower temperatures, a decreased magnetic moment is obtained, as is usually the case with Ce misfit-layered compounds such as  $(\text{CeS})_{1.15}\text{NbS}_2$ .<sup>27</sup>

Although the temperature dependence of the magnetic susceptibility of the  $(\text{CeS})_{1.15}(\text{TaS}_2)_2(\text{CoCp}_2)_{0.31}$  intercalate is similar to that of the host, the temperature-independent component term is significantly larger. The plots, Figure 4a,b, also exhibit a subtle slope change at about 270 K that is more outstanding in the inverse susceptibility plot (Figure 4 b) and can be ascribed to at least two effects, namely, the presence of small amounts of some ferromagnetic impurity (e.g. Co particles) otherwise undetected by XRD or XPS techniques or an experimental artifact (at high temperatures, SQUID measurements occasionally result in shoulders such as that exhibited by the intercalate above 270 K, the origin of which has been related to expansion of the sample holder). In fact, we used different magnetic fields for magnetic susceptibility measurements and observed a linear relationship between  $M$  and  $H$  over a range of 10 kOe and 5 K; we can thus conclude that any ferromagnetic impurity is below the detection level of the SQUID magnetometer. The final magnetic susceptibility data were recorded at 1 kOe. The slope change in the  $\chi$  vs  $T$  plot therefore appears to result from intrinsic experimental factors, so the discussion of magnetic data is restricted to temperatures below 270 K.

The magnetic moment of the intercalate at high temperatures is significantly larger than that obtained for the host (which is quite coincident with the theoretical value for  $\text{Ce}^{3+}$ ). Better consistency between the magnetic moments of both compounds is obtained by taking into account the increase in Pauli paramagnetism upon intercalation. This temperature-independent term was estimated to be  $4.94 \times 10^{-6}$  emu/g from a  $\chi T$  vs  $T$  plot above 200 K. The corrected values are also shown in Figure 4b; an effective moment of  $2.60 \mu_B$  was obtained over the 100–200 K range which is similar to

(22) Ettema, A. Ph.D. Thesis, University of Groningen, Groningen, The Netherlands, 1993.

(23) Manova, E.; Leautic, A.; Mitov, I.; Gombeau, D.; Clement, R. *Mol. Cryst. Liq. Cryst.* **1998**, *311*, 155.

(24) O'Hare, D.; Jaegermann, W.; Williamson, D. L.; Ohuchi, F. S.; Parkinson, B. A. *Inorg. Chem.* **1988**, *27*, 1537.

(25) Espinós, J. P.; González-Elipe, A. R.; Hernán, L.; Morales, J.; Sánchez, L.; Santos, J. *Surf. Sci.* **1999**, *426*, 259.

(26) Wiegers, G. A.; Meetsma, A.; Haange, R. J.; de Boer, J. L. *J. Solid State Chem.* **1990**, *89*, 328.

(27) Peña, O.; Meerschaut, A.; Rabu, P. *J. Magn. Magn. Mater.* **1992**, *104–107*, 1249.

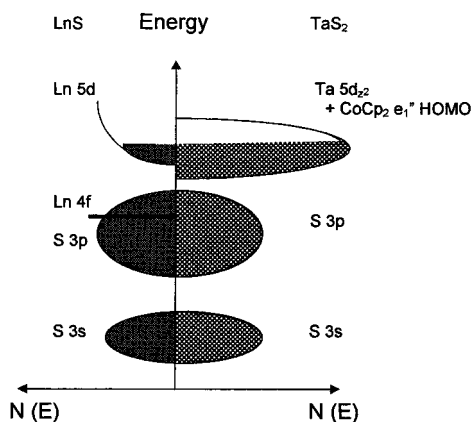


**Figure 5.** Schematic density of state vs energy diagram of rare earth misfit layer compound, taken from ref 29, intercalated with cobaltocene.

that calculated for the pristine compound. These results also provide direct evidence that the cobaltocene molecule is intercalated mainly as cobaltocenium ion, a diamagnetic species, the loss of moment being consistent with the transfer of one electron from the guest molecule to the  $\text{TaS}_2$  part of the host. In fact, this intercalation model is adhered to in the  $\text{TaS}_2(\text{CoCp}_2)_{0.25}$  and  $(\text{PbS})_{1.14}(\text{TaS}_2)_2(\text{CoCp}_2)_{0.28}$  intercalates.<sup>20,28</sup>

The more complex magnetic behavior shown by the Sm system precludes a clear-cut description of the way it is influenced by the intercalation of cobaltocene. In fact, the magnetic properties of this ion are not dictated solely by its ground-state configuration; rather, the thermal energy is high enough to promote some electrons and to partially populate the higher state. Different magnetic measurements are in progress to obtain insight into the problem of admixtures of energy states and the fluctuation population caused by the intercalant.

The electron transfer can be discussed in terms of the band structure proposed to account for the electronic properties of these composites. Figure 5 shows the variation of the density of states, taken from ref 29, as a function of energy. This model accounts fairly well for the photoelectron spectra and electrical transport properties of monolayer Ln-based misfit layer sulfides. The figure has been adapted to account for the composition  $(\text{CeS})_{0.57}\text{TaS}_2$  where formally an electron transfer of about 0.5 e/Ta atom takes place, on the assumption that the lanthanides are trivalent, and where it is transferred to the  $\text{TaS}_2$  layers. This donation should result in a  $d_{z^2}$  band of the  $\text{TaS}_2$  more than half filled. Wiegiers et al.<sup>29</sup> also suggested the presence of a conduction band of mainly 5d of Ln, partly filled, because a small fraction of electron is not transferred from the LnS double layer to the  $\text{TaS}_2$  sandwiches. The presence of virtually a single oxidation state of cobaltocene ( $\text{CoCp}_2^+$ ) intercalated in the chalcogenide indicates that the reduction potential of cobaltocene is above to the Fermi level of the host and that the electron transfer would take place

through overlap of the lowest unoccupied d-band levels with the highest occupied orbitals of cobaltocene (anti-bonding  $e_1''$  orbitals). The overall driving force of the intercalation reaction must thus be a redox process defined by the difference in the electrochemical potentials of the electrons in the solid defined by the Fermi level and the guest. From such a simple scheme, one can expect the electron donation to lead to a decrease in the total density of states,  $N(E_F)$ , thus decreasing the magnetic susceptibility of the intercalate. However, the observed values are slightly greater than that of the pristine host, which may have resulted from contamination of  $\text{CoCp}_2$  probably adsorbed at level surface. In fact, the presence of tails at the low binding energy side of the Co 2p photoemission peaks may account for that of a cobalt species as a neutral molecule. In any case, the intercalation of molecular guest species is a complex process and the overall free energy of the system may be governed by other factors. Thus, an ionic model has been used to explain the unusual arrangement of the  $\text{NH}_3$  molecule in the  $\text{TaS}_2\cdot\text{NH}_3$  system<sup>30</sup> (with the  $C_3$  axis parallel to the sulfur layers). In the composition suggested,  $(\text{NH}_4^+)_x(\text{NH}_3)_{1-x}[\text{TaS}_2]^{x-}$ , solvation of  $\text{NH}_4^+$  by neutral molecules plays a relevant role. In our case, the amount of cointercalated solvent is negligible and solvation effects must contribute little to stabilizing the intercalate. Bearing in mind the difficulty in having an accurate model explain bonding between the guest and the host lattice, from the foregoing it seems quite clear that the intercalation of cobaltocene into lanthanide-based misfit layer sulfides can be described in terms of a redox reaction that leads to the formation of a cationic guest species, the lanthanide element remaining as a trivalent cation.

## Conclusions

The above results show that electron-rich organometallic guests such as cobaltocene can be intercalated into lanthanide-based misfit-layered sulfides under mild-temperature conditions. This reaction is accompanied by electron transfer from the intercalant to the  $\text{TS}_2$  layered sublattice, which is compatible with electron donation from the MS part to the  $\text{TS}_2$  one. In fact, in formal terms, misfit-layered chalcogenides themselves can be considered to be intercalated phases of transition metal dichalcogenides and concepts such as charge transfer from one subsystem to the other (as in  $\text{TX}_2$  intercalates) apply here. On the other hand, these results reveal that the ability of this family of composite materials to undergo intercalation reactions can be explained in simple terms, a redox reaction and ion formation, similarly to binary layered sulfides.

**Acknowledgment.** The authors gratefully acknowledge financial support from Spain's CICYT (Project PB95-0561) and Junta de Andalucía (Group FQM 0175).

CM0010396

(28) Morales, J.; Santos, J.; Baas, J.; Wiegiers, G. A.; Martínez, J. L. *Chem. Mater.* **1999**, *11*, 2737.

(29) Zhou, W. Y.; Meetsma, A.; de Boer, J. L.; Wiegiers, G. A. *J. Alloys Compd.* **1996**, *233*, 80.

(30) Schöllhorn, R.; Zagefka, H. D. *Angew. Chem., Int. Ed. Engl.* **1977**, *16*, 199.